

Learn to Predict Sets Using Feed-Forward Neural Networks

Hamid Rezatofighi, Roman Kaskman, Farbod T. Motlagh, Qinfeng Shi,
Anton Milan, Daniel Cremers, Laura Leal-Taixé, Ian Reid

Abstract—This paper addresses the task of set prediction using deep feed-forward neural networks. A set is a collection of elements which is invariant under permutation and the size of a set is not fixed in advance. Many real-world problems, such as image tagging and object detection, have outputs that are naturally expressed as sets of entities. This creates a challenge for traditional deep neural networks which naturally deal with structured outputs such as vectors, matrices or tensors. We present a novel approach for learning to predict sets with unknown permutation and cardinality using deep neural networks. In our formulation we define a likelihood for a set distribution represented by a) two discrete distributions defining the set cardinality and permutation variables, and b) a joint distribution over set elements with a fixed cardinality. Depending on the problem under consideration, we define different training models for set prediction using deep neural networks. We demonstrate the validity of our set formulations on relevant vision problems such as: 1) multi-label image classification where we achieve state-of-the-art performance on the PASCAL VOC and MS COCO datasets, 2) object detection, for which our formulation outperforms state-of-the-art detectors such as Faster R-CNN and YOLO v3, and 3) a complex CAPTCHA test, where we observe that, surprisingly, our set-based network acquired the ability of mimicking arithmetics without any rules being coded.

Index Terms—Random Finite set, Deep learning, Unstructured data, Permutation, Image tagging, Object detection, CAPTCHA.

1 INTRODUCTION

DEEP structured networks such as deep convolutional (CNN) and recurrent (RNN) neural networks have enjoyed great success in many real-world problems, including scene classification [1], semantic segmentation [2], speech recognition [3], gaming [4], [5], and image captioning [6]. However, the current configuration of these networks is restricted to accept and predict structured inputs and outputs such as vectors, matrices, and tensors. If the problem’s inputs and/or outputs cannot be modelled in this way, all these learning approaches fail to learn a proper model [7]. However, many real-world problems are naturally described as unstructured data such as sets [7], [8]. A set is a collection of elements which is *invariant under permutation* and the size of a set is *not fixed* in advance. Set learning using deep networks has generated substantial interest very recently [7], [8], [9], [10], [11], [12], [13].

Consider the task of image classification as an example. The goal here is to predict a label (or a category) of a given image. The most successful approaches address this task with CNNs, *i.e.* by applying a series of convolutional layers followed by a number of fully connected layers [1], [14], [15], [16]. The final output layer is a fixed-sized vector with the length corresponding to the number of categories in the dataset (*e.g.* 1000 in the case of the ILSVRC Challenge [17]). Each element in this vector is a score or probability for one particular category such that the final prediction corresponds to an approximate probability distribution over all classes. The difficulty arises when the number of class labels is unknown in advance and in particular varies for each example.

Then, the final output is generated heuristically by a discretization process such as choosing the k highest scores [18], [19], which is not part of the learning process. We argue that this problem should be naturally formulated as prediction of the sets of labels where the output does not have any known or fixed ordering or cardinality.

As a second example, let us consider the task of object detection. Given a structured input, *e.g.* an image as a tensor, the goal is to predict a set of *orderless* locations, *e.g.* bounding boxes, from an unknown and varying number of objects. Therefore, the output of this problem can be properly modelled as a set of entities. However, a typical deep learning network cannot be simply trained to directly predict a varying number of orderless locations. Existing approaches formulate this problem using a pre-defined and fixed-sized grid [20], [21] or anchor boxes [22] representing a coarse estimate of all possible locations and scales of objects. Then, each location and scale is scored independently to determine whether or not it contains an object. The final output is generated heuristically by a discretization process such as non-maximum suppression (NMS), which is not part of the learning process.¹ Therefore, their performance is hindered by this heuristic procedure. This is one reason why current solutions can only deal with moderate object occlusion. We argue that object detection should rather be posed as a set prediction problem, where a deep learning network is trained to output a *set* of locations without any heuristics.

This shortcoming does not only concern object detection but also all problems where a set of instances as input and/or output is involved. Other examples of such tasks include predicting a set of topics or concepts in documents [25], sets of points in point cloud data [26], [27], [28], segmentation of object instances [29]

• Hamid Rezatofighi, Farbod T. Motlagh, Qinfeng Shi, and Ian Reid are with the School of Computer Science, The University of Adelaide, Australia.
E-mail: hamid.rezatofighi@adelaide.edu.au

• Anton Milan is with Amazon. This work was done prior to joining Amazon.

• Roman Kaskman, Daniel Cremers, and Laura Leal-Taixé, are with Technical University of Munich, Germany.

1. Recently, [23], [24] have attempted to learn this process. However they assume the relationship between bounding boxes to be pairwise only. Moreover, an additional pairwise network is introduced on top of the detection network to learn these pairwise relationships, which may be computationally prohibitive.

and a set of trajectories in multiple object tracking [30], [31], [32]. In contrast to problems such as classification, where the order of categories or the labels can be fixed during the training process and the output can be well represented by a fixed-sized vector, the instances are often unfixed in number and orderless. More precisely, it does not matter in which order the instances are labelled and these labels do not relate the instances to a specific visual category. To this end, training a deep network to input or predict instances seems to be non-trivial. We believe that set learning is a principled solution to all of these problems.

In this paper, we present a novel approach for learning to deal with sets using deep learning. More clearly, in the presented model, we assume that the input (the observation) is still structured, *e.g.* an image, but the annotated outputs are available as a set of labels. This paper is a both technical and experimental extension of our recent works on set learning using deep neural networks [8], [9]. Although our work in [8], [9] handles orderless outputs in the testing/inference step, it assumes that the annotated labels can be ordered in the learning step. This might be suitable for the problems such as multi-label image classification problem. However, many applications, such as object detection, the output labels cannot be naturally ordered in an structure way during training. Therefore, our model introduced in [8], [9] cannot learn a sensible model for truly orderless problems such as object detection (see Sec. 4.2 for the experiment). In this paper in addition to what we proposed in [8], [9], we also propose a complete set prediction formulation to address this limitation (*cf.* **Scenario 2** and **Scenario 3** in Sec. 3.2). This provides a potential to tackle many other set prediction problems compared to [8], [9]. To this end, in addition to multi-label image classification, we test this complete model on two new problems, *i.e.* object detection and CAPTCHA test.

Compared to our previous work [8], [9], the additional contribution of the paper is summarised as follows:

- 1) We provide a complete formulation for neural networks to deal with arbitrary sets with unknown permutation and cardinality as available annotated outputs. This makes a feed-forward neural network able to truly handle set outputs at both training and test time.
- 2) Additionally, this new formulation allows us to learn the distribution over the unobservable permutation variables, which can be used to identify if there exist any natural ordering for the annotated labels. In some applications, there may exist one or several dominant orders, which are unknown from the annotations.
- 3) We reformulate object detection as a set prediction problem, where a deep network is learned end-to-end to generate the detection outputs with no heuristic involved. We outperform the state-of-the-art object detectors, such as Faster R-CNN and YOLO v3, on both simulated and a small-scale real data with high level of occlusions.
- 4) We also demonstrate the applicability of our framework algorithm for a complex CAPTCHA test which can be formulated as a set prediction problem.

2 RELATED WORK

Handling unstructured input and output data, such as sets or point patterns, for both learning and inference is an emerging field of study that has generated substantial interest in recent years. Approaches such as mixture models [25], [33], [34], learning distributions from a set of samples [35], [36], model-based multiple

instance learning [37], and novelty detection from point pattern data [38], can be counted as few out many examples that use point patterns or sets as input or output and directly or indirectly model the set distributions. However, existing approaches often rely on parametric models, *e.g. i.i.d.* Poisson point or Gaussian Process assumptions [38], [39]. Recently, deep learning has enabled us to use less parametric models to capture highly complex mapping distributions between structured inputs and outputs. This learning framework has demonstrated its great success in addressing pixel-to-pixel (or tensor-to-tensor) problems. There has been recently few attempts to apply this successful learning framework for the other types of data structures such as sets. One of earliest works in this direction is the work of [10], which uses an RNN to read and predict sets. However, the output is still assumed to have a single order, which contradicts the orderless property of sets. Moreover, the framework can be used in combination with RNNs only and cannot be trivially extended to any arbitrary learning framework such as feed-forward architectures. Generally speaking, the sequential techniques *e.g.* RNN, LSTM and GRU, can deal with variable input or output sizes. However, they learn the parameters of a model for conditionally dependent inputs and outputs according to a chain rule; regardless if their orders assumed to be known or unknown during the training process [10]. To this end, these sequential learning techniques may not be an appropriate choice for encoding and decoding sets.

Alternatively the feed-forward neural networks has been recently attempted to be applied for inputting or outputting sets. Most existing approaches on set learning [7], [11], [12] have focused on the problem of encoding a set with a feed-forward neural network by using, *e.g.* a shared network followed by a symmetrical pooling function [7], a permutation invariant pooling layer [11] or a permutation invariant representation for sets [12]. The similar concepts has been independently developed by the community working to encode point clouds using feed-forward neural networks [26], [27]. However, in all these works, the outputs of neural networks are either assumed to be a tensor or a set with the same entities of the input set, which prevents this approach to be used for the problems that require output sets with arbitrary entities. In this paper, we are instead interested in learning a model to output an arbitrary set. Somewhat surprisingly, there are only few works on learning to predict sets using deep neural networks [8], [9], [13]. The most related work to our problem is our previously proposed framework [8] which seamlessly integrates a deep learning framework into set learning in order to learn to output sets. However, the approach only formulates the outputs with unknown cardinality and does not consider the permutation variables of sets in the learning step. Therefore, its application is limited to the problems with a fixed order output such as image tagging and diverges when trying to learn unordered output sets as for the object detection problem. In this paper, we incorporate these permutations as unobservable variables in our formulation, and estimate their distribution during the learning process. Our unified set prediction framework has the potential to reformulate some of the existing problems, such as object detection, and to tackle a set of new applications, such as a logical CAPTCHA test which cannot be trivially solved by the existing architectures.

3 DEEP PERM-SET NETWORK

A set is a collection of elements which is invariant under permutation and the size of a set is not fixed in advance, *i.e.*

TABLE 1: All mathematical symbols and notations used throughout the paper.

Symbol/Notation	Definition
m	Cardinality variable
π	Permutation variable
$\boldsymbol{\pi}$ or $(\pi_1, \pi_2, \dots, \pi_m)$	Permutation vector for m elements
\mathbb{N}^*	Space of all non-negative integer numbers
$\boldsymbol{\Pi}$ or $\{\boldsymbol{\pi}_1, \boldsymbol{\pi}_2, \dots, \boldsymbol{\pi}_{m!}\}$	Space of all feasible permutations for a vector with cardinality m
\mathcal{Y} or $\{\mathbf{y}_1, \dots, \mathbf{y}_m\}$	Set with unknown permutation and cardinality
\mathcal{Y}^m or $\{\mathbf{y}_1, \dots, \mathbf{y}_m\}^m$	Set with unknown permutation, but known cardinality
$\mathbf{Y}_{\boldsymbol{\pi}}^m$ or $(\mathbf{y}_{\pi_1}, \dots, \mathbf{y}_{\pi_m})$	Set with known permutation and cardinality (or a tensor)
\mathbf{x}	Input data as a tensor (<i>e.g.</i> an RGB image)
\mathbf{w}	Collection of model parameters (<i>e.g.</i> all deep neural network parameters)
\mathcal{D} or $\{(\mathbf{x}_i, \mathcal{Y}_i)\}$	Training dataset
U	Unit of hyper-volume in the feature space
$p(m)$	Distribution over the cardinality variable m (a discrete distribution)
$p_m(\cdot)$	Joint distribution of m variables (m is known)

$\mathcal{Y} = \{\mathbf{y}_1, \dots, \mathbf{y}_m\}$, $m \in \mathbb{N}^*$. A statistical function describing a finite-set variable \mathcal{Y} is a combinatorial probability density function $p(\mathcal{Y})$ defined by $p(\mathcal{Y}) = p(m)U^m p_m(\{\mathbf{y}_1, \mathbf{y}_2, \dots, \mathbf{y}_m\})$, where $p(m)$ is the cardinality distribution of the set \mathcal{Y} and $p_m(\{\mathbf{y}_1, \mathbf{y}_2, \dots, \mathbf{y}_m\})$ is a symmetric joint probability density distribution of the set given known cardinality m . U is the unit of hyper-volume in the feature space, which cancels out the unit of the probability density $p_m(\cdot)$ making it unit-less, and thereby avoids the unit mismatch across the different dimensions (cardinalities) [37].

Throughout the paper, we use $\mathcal{Y} = \{\mathbf{y}_1, \dots, \mathbf{y}_m\}$ for a set with unknown cardinality and permutation, $\mathcal{Y}^m = \{\mathbf{y}_1, \dots, \mathbf{y}_m\}^m$ for a set with known cardinality m but unknown permutation and $\mathbf{Y}_{\boldsymbol{\pi}}^m = (\mathbf{y}_{\pi_1}, \dots, \mathbf{y}_{\pi_m})$ for an ordered set with known cardinality (or dimension) m and permutation $\boldsymbol{\pi}$, which means that the m set elements are ordered under the permutation vector $\boldsymbol{\pi} = (\pi_1, \pi_2, \dots, \pi_m)$. Note that an ordered set with known dimension and permutation exactly corresponds to a tensor, *e.g.* a vector or a matrix.

According to the permutation invariant property of the sets, the set \mathcal{Y}^m with known cardinality m can be expressed by an ordered set with any arbitrary permutation, *i.e.* $\mathcal{Y}^m := \{\mathbf{Y}_{\boldsymbol{\pi}}^m | \forall \boldsymbol{\pi} \in \boldsymbol{\Pi}\}$, where, $\boldsymbol{\Pi}$ is the space of all feasible permutation $\boldsymbol{\Pi} = \{\boldsymbol{\pi}_1, \boldsymbol{\pi}_2, \dots, \boldsymbol{\pi}_{m!}\}$ and $|\boldsymbol{\Pi}| = m!$. Therefore, the probability density of a set \mathcal{Y} with unknown permutation and cardinality conditioned on the input \mathbf{x} and the model parameters \mathbf{w} is defined as

$$\begin{aligned} p(\mathcal{Y}|\mathbf{x}, \mathbf{w}) &= p(m|\mathbf{x}, \mathbf{w}) \times U^m \times p_m(\mathcal{Y}^m|\mathbf{x}, \mathbf{w}), \\ &= p(m|\mathbf{x}, \mathbf{w}) \times U^m \times \sum_{\forall \boldsymbol{\pi} \in \boldsymbol{\Pi}} p_m(\mathbf{Y}_{\boldsymbol{\pi}}^m, \boldsymbol{\pi}|\mathbf{x}, \mathbf{w}). \end{aligned} \quad (1)$$

The parameter vector \mathbf{w} models both the *cardinality* distribution of the set elements $p(m|\cdot)$ as well as the joint state distribution of set elements and their *permutation* for a fixed cardinality $p_m(\mathbf{Y}_{\boldsymbol{\pi}}^m, \boldsymbol{\pi}|\cdot)$.

The above formulation represents the probability density of a set which is very general and completely independent of the choices of cardinality, state and permutation distributions. It is thus straightforward to transfer it to many applications that require the output to be a set. Definition of these distributions for the applications in this paper will be elaborated later.

3.1 Posterior distribution

Let $\mathcal{D} = \{(\mathbf{x}_i, \mathcal{Y}_i)\}$ be a training set, where each training sample $i = 1, \dots, n$ is a pair consisting of an input feature (*e.g.* image),

$\mathbf{x}_i \in \mathbb{R}^l$ and an output set $\mathcal{Y}_i = \{\mathbf{y}_1, \mathbf{y}_2, \dots, \mathbf{y}_{m_i}\}$, $\mathbf{y}_k \in \mathbb{R}^d$, $m_i \in \mathbb{N}^*$. The aim is now to learn the parameters \mathbf{w} to estimate the set distribution in Eq. (1) using the training samples.

To learn the parameters \mathbf{w} , we assume that the training samples are independent from each other and the distribution $p(\mathbf{x})$ from which the input data is sampled is independent from both the output and the parameters. Then, the posterior distribution over the parameters can be derived as

$$\begin{aligned} p(\mathbf{w}|\mathcal{D}) &\propto p(\mathcal{D}|\mathbf{w})p(\mathbf{w}) \\ &\propto \prod_{i=1}^n \left[p(m_i|\mathbf{x}_i, \mathbf{w}) \times U^{m_i} \times \sum_{\forall \boldsymbol{\pi} \in \boldsymbol{\Pi}} p_m(\boldsymbol{\pi}|\mathbf{x}_i, \mathbf{w}) \right. \\ &\quad \left. \times p_m(\mathbf{Y}_{\boldsymbol{\pi}}^{m_i}|\mathbf{x}_i, \mathbf{w}, \boldsymbol{\pi}) \right] p(\mathbf{w}). \end{aligned}$$

Note that $p_m(\mathbf{Y}_{\boldsymbol{\pi}}^{m_i}, \boldsymbol{\pi}|\cdot)$ is decomposed according to the chain rule and $p(\mathbf{x})$ is eliminated as it appears in both the numerator and the denominator. We also assume that the outputs in the set are derived from an independent and identically distributed (*i.i.d.*) cluster point process model. Therefore, the full posterior distribution can be written as

$$\begin{aligned} p(\mathbf{w}|\mathcal{D}) &\propto \prod_{i=1}^n \left[p(m_i|\mathbf{x}_i, \mathbf{w}) \times U^{m_i} \times \right. \\ &\quad \left. \sum_{\forall \boldsymbol{\pi} \in \boldsymbol{\Pi}} \left(p_m(\boldsymbol{\pi}|\mathbf{x}_i, \mathbf{w}) \times \prod_{\sigma=\pi_1}^{\pi_{m_i}} p(\mathbf{y}_\sigma|\mathbf{x}_i, \mathbf{w}, \boldsymbol{\pi}) \right) \right] p(\mathbf{w}). \end{aligned} \quad (2)$$

We would like to re-emphasize that the assumption here is that the annotated labels, \mathcal{Y}_i , are available as a set of entities, *e.g.* a set of image tags or bounding boxes, and this means that we might not have any knowledge if there exist any natural ordering structure in the data. Our proposed solution is capable of inferring these potential ordering structures (if they exist at all) in the data by learning the distribution over the permutations, *i.e.* $p_m(\boldsymbol{\pi}|\cdot, \cdot)$. We can also assume that $p_m(\boldsymbol{\pi}|\cdot, \cdot)$ is uniform over all permutations (*i.e.* the order does not matter) and learn the model accordingly. Moreover, in some applications, *e.g.* image tagging, we can assume that the permutation of the outputs for all the training data for the training stage can be consistently fixed. Therefore, in this case the permutation is not a random variable and will be eliminated from the posterior distribution. The learning process for each of these scenarios is slightly different, therefore, in the next section we detail them as Scenarios 1, 2 and 3.

3.2 Learning

For learning the parameters in the aforementioned scenarios, we use a point estimate for the posterior, *i.e.* $p(\mathbf{w}|\mathcal{D}) = \delta(\mathbf{w} = \mathbf{w}^*|\mathcal{D})$, where \mathbf{w}^* is computed using the MAP estimator, *i.e.* $\mathbf{w}^* = \arg \min_{\mathbf{w}} -\log(p(\mathbf{w}|\mathcal{D}))$. Since \mathbf{w} in this paper is assumed to be the parameters of a deep neural network, to estimate \mathbf{w}^* , we use commonly used stochastic gradient decent (SGD), where one iteration is performed as $\mathbf{w}_k = \mathbf{w}_{k-1} - \eta \frac{-\partial \log(p(\mathbf{w}_{k-1}|\mathcal{D}))}{\partial \mathbf{w}_{k-1}}$, where η is the learning rate.

3.2.1 Scenario 1: Permutation can be fixed during training

In some problems, although the output labels represent a set (without any preferred ordering), during training step they can be consistently ordered in an structure way. For example, in multi-label image classification problem, all possible tags can be ordered in an arbitrary way, *e.g.* (Person, Dog, Bike, ...) or (Dog, Person, Bike, ...), but they can be fixed to be the exactly same order for all training instances during training step.

In this scenario, since π is not a random variable in this case, $p(\mathbf{y}_\sigma|\mathbf{x}_i, \mathbf{w}, \pi) = p(\mathbf{y}_\sigma|\mathbf{x}_i, \mathbf{w})$. Therefore the term $p_m(\pi|\cdot, \cdot)$ is marginalized out from the posterior distribution

$$p(\mathbf{w}|\mathcal{D}) \propto \prod_{i=1}^n \left[p(m_i|\mathbf{x}_i, \mathbf{w}) \times U^{m_i} \times \prod_{\sigma=1}^{m_i} p(\mathbf{y}_\sigma|\mathbf{x}_i, \mathbf{w}) \times \underbrace{\sum_{\forall \pi \in \Pi} (p_m(\pi|\mathbf{x}_i, \mathbf{w}))}_{=1} \right] p(\mathbf{w}), \quad (3)$$

and it is simplified as

$$p(\mathbf{w}|\mathcal{D}) \propto \prod_{i=1}^n \left[p(m_i|\mathbf{x}_i, \mathbf{w}) \times U^{m_i} \times \prod_{\sigma=1}^{m_i} p(\mathbf{y}_\sigma|\mathbf{x}_i, \mathbf{w}) \right] p(\mathbf{w}). \quad (4)$$

Therefore, for learning the parameters of a neural network \mathbf{w} , we have

$$\begin{aligned} \mathbf{w}^* &= \arg \min_{\mathbf{w}} -\log(p(\mathbf{w}|\mathcal{D})), \\ &= \arg \min_{\mathbf{w}} \sum_{i=1}^n \left[\underbrace{-\log(p(m_i|\mathbf{x}_i, \mathbf{w}))}_{\mathcal{L}_{card}(\cdot)} - \underbrace{m_i \log U}_{\text{removed}} \right] \\ &\quad + \sum_{\sigma=1}^{m_i} \left(\underbrace{-\log(p(\mathbf{y}_\sigma|\mathbf{x}_i, \mathbf{w}))}_{\mathcal{L}_{state}(\cdot)} \right) + \gamma \|\mathbf{w}\|_2^2, \end{aligned} \quad (5)$$

$$\begin{aligned} \mathbf{w}^* &= \arg \min_{\mathbf{w}} \sum_{i=1}^n \left[\mathcal{L}_{card}(m_i, \alpha(\mathbf{x}_i, \mathbf{w})) + \right. \\ &\quad \left. \sum_{\sigma=1}^{m_i} \left(\mathcal{L}_{state}(\mathbf{y}_\sigma, \mathbf{O}_1^\sigma(\mathbf{x}_i, \mathbf{w})) \right) \right] + \gamma \|\mathbf{w}\|_2^2. \end{aligned} \quad (6)$$

where γ is the regularisation parameter, which is also known as the weight decay parameter and is commonly used in training neural networks. $\mathcal{L}_{card}(\cdot, \alpha(\cdot, \cdot))$ and $\mathcal{L}_{state}(\cdot, \mathbf{O}_1^\sigma(\cdot, \cdot))$ represent cardinality and state losses, respectively, where $\alpha(\cdot, \cdot)$ and $\mathbf{O}_1^\sigma(\cdot, \cdot)$ are respectively the part of output layer of the neural network, which predict the cardinality and the state of each of m_i set elements.

Implementation insight: In this scenario, the training procedure is simplified to jointly optimize cardinality $\mathcal{L}_{card}(\cdot, \alpha(\cdot, \cdot))$

and state $\mathcal{L}_{state}(\cdot, \mathbf{O}_1^\sigma(\cdot, \cdot))$ losses under a pre-fixed permutation of output labels².

The cardinality loss, $\mathcal{L}_{card}(\cdot, \alpha(\cdot, \cdot))$, can be the negative log of any discrete distribution such as Poisson, binomial, negative binomial, categorical (softmax) or Dirichlet-categorical (*cf.* [8], [9], [40]). Therefore, $\alpha(\cdot, \cdot)$ represents the parameters of this discrete distribution, *e.g.* a single parameter for Poisson or $M+1$ parameters (*i.e.* $M+1$ event probabilities for set with maximum cardinality M) for a categorical distribution. We will compare some of those cardinality losses for the image tagging problem in Sec. 4.

For the state loss, $\mathcal{L}_{state}(\cdot, \mathbf{O}_1^\sigma(\cdot, \cdot))$, with variable output set cardinality, we assume that the maximum set cardinality to be generated is known. This would be a practical assumption for some applications, *e.g.* image tagging, where the output set is always a subset of the maximum sized set with all pre-defined M labels, *i.e.* $\mathcal{Y} \subseteq \{\ell_1, \ell_2, \dots, \ell_M\}$. Therefore, the output of the network for this part would be the collection of the states and existence score for all M set elements, *i.e.* $\mathbf{O}_1 = (\mathbf{O}_1^1, \mathbf{O}_1^2, \dots, \mathbf{O}_1^M)$. In image tagging, the state loss, $\mathcal{L}_{state}(\cdot, \mathbf{O}_1^\sigma(\cdot, \cdot))$ can be simply a loss defined over the predicted existence score for each M labels in an image, *e.g.* a logistic regression or binary cross entropy (BCE) loss. Remember that, in this scenario, the assignment of the truth (labels in image tagging) to the index of the outputs is known and fixed during training.

3.2.2 Scenario 2: Learning the distribution over the permutations

In the problems, where the outputs are set of instances, instead of a set of categories or classes, similar to the previous scenario, we cannot create a consistent fixed ordering representation for all instances during training procedure.

In this scenario, we assume that the permutation cannot be fixed at training time. Therefore, the posterior distribution is exactly as defined in Eq. (2). For learning the parameters and in order to optimize the negative logarithm of the posterior over the parameters, *i.e.* $-\log(p(\mathbf{w}|\mathcal{D}))$, we need to marginalize over all permutations in every iteration of SGD, which is combinatorial and can become intractable even for relatively small-sized problems. To address this, we approximate this marginalization with the most significant permutations (the permutation samples with high probability) for each training instance from the samples attained in each iteration of SGD, *i.e.*

$$\begin{aligned} p_m(\pi|\mathbf{x}_i, \mathbf{w}) &= \sum_{\forall \pi \in \Pi} \omega_\pi(\mathbf{x}_i, \mathbf{w}) \delta(\pi) \\ &\approx \frac{1}{N_\kappa} \sum_{\forall \pi_{i,k}^* \in \Pi} \tilde{\omega}_{\pi_{i,k}^*}(\mathbf{x}_i, \mathbf{w}) \delta(\pi_{i,k}^*), \end{aligned} \quad (7)$$

where $\delta(\cdot)$ is the Kronecker delta and $\sum_{\forall \pi \in \Pi} \omega_\pi(\cdot, \cdot) = 1$. $\pi_{i,k}^*$ is the most significant permutation for the training instance i , sampled from $p_m(\pi|\cdot, \cdot) \times \prod_{\sigma=1}^{m_i} p(\mathbf{y}_\sigma|\cdot, \cdot, \pi)$ during k^{th} iteration of SGD (using Eq. 9). The weight $\tilde{\omega}_{\pi_{i,k}^*}(\cdot, \cdot)$ is proportional to the number of the same permutation samples $\pi_{i,k}^*(\cdot, \cdot)$, extracted during all SGD iterations for the training instance i and N_κ is the total number of SGD iterations. Therefore, $\sum_{\forall \pi_{i,k}^* \in \Pi} \tilde{\omega}_{\pi_{i,k}^*}(\cdot, \cdot) / N_\kappa = 1$. Note that at every iteration, as the parameter vector \mathbf{w} is updated, the best permutation $\pi_{i,k}^*$ can change accordingly even for the same instance \mathbf{x}_i . This allows the network to traverse through the entire space Π and to approximate

2. This is only possible for some applications, where the outputs are category or class labels rather than instance labels, *e.g.* multi-label image classification.

$p_m(\pi|\mathbf{x}_i, \mathbf{w})$ by a set of significant permutations. To this end, $p_m(\pi|\mathbf{x}_i, \mathbf{w})$ is assumed to be point estimates for each iteration of SGD. Therefore,

$$\begin{aligned} p(\mathbf{w}_k|\mathcal{D}) &\approx \prod_{i=1}^n \left[p(m_i|\mathbf{x}_i, \mathbf{w}_k) \times U^{m_i} \times \tilde{\omega}_{\pi_{i,k}^*}(\mathbf{x}_i, \mathbf{w}_k) \right. \\ &\quad \left. \times \prod_{\sigma=\pi_1}^{\pi_{m_i}} p(\mathbf{y}_\sigma|\mathbf{x}_i, \mathbf{w}_k, \pi_{i,k}^*) \right] p(\mathbf{w}_k). \end{aligned} \quad (8)$$

In summary, to learn the parameters of the network \mathbf{w} , the best permutation sample for each instance i in each SGD iteration k , *i.e.* $\pi_{i,k}^*$ is attained by solving the following assignment problem, first:

$$\begin{aligned} \pi_{i,k}^* &= \arg \min_{\pi \in \Pi} -\log \left(p_m(\pi|\cdot, \cdot) \times \prod_{\sigma=\pi_1}^{\pi_{m_i}} p(\mathbf{y}_\sigma|\cdot, \cdot, \pi) \right) \\ &= \arg \min_{\pi \in \Pi} \mathcal{L}_{perm}(\pi, \mathbf{O}_2(\mathbf{x}_i, \mathbf{w}_{k-1})) \\ &\quad + \sum_{\sigma=\pi_1}^{\pi_{m_i}} \left(\mathcal{L}_{state}(\mathbf{y}_\sigma, \mathbf{O}_1^\sigma(\mathbf{x}_i, \mathbf{w}_{k-1})) \right), \end{aligned} \quad (9)$$

and then use the sampled permutation $\pi_{i,k}^*$ to apply standard back-propagation as follows:

$$\begin{aligned} \mathbf{w}_k &= \mathbf{w}_{k-1} - \eta \frac{-\partial \log(p(\mathbf{w}_{k-1}|\mathcal{D}))}{\partial \mathbf{w}_{k-1}} \\ &= \mathbf{w}_{k-1} - \eta \sum_{i=1}^n \left[\frac{\partial \mathcal{L}_{card}(m_i, \alpha)}{\partial \alpha} \cdot \frac{\partial \alpha}{\partial \mathbf{w}} + \right. \\ &\quad \left. \frac{\partial \mathcal{L}_{perm}(\pi_{i,k}^*, \mathbf{O}_2)}{\partial \mathbf{O}_2} \cdot \frac{\partial \mathbf{O}_2}{\partial \mathbf{w}} + \right. \\ &\quad \left. \sum_{\sigma=\pi_1^*}^{\pi_{m_i}^*} \frac{\partial \mathcal{L}_{state}(\mathbf{y}_\sigma, \mathbf{O}_1^\sigma)}{\partial \mathbf{O}_1^\sigma} \cdot \frac{\partial \mathbf{O}_1^\sigma}{\partial \mathbf{w}} \right] + 2\gamma \mathbf{w}, \end{aligned} \quad (10)$$

where $\mathcal{L}_{card}(\cdot, \alpha(\cdot, \cdot))$, $\mathcal{L}_{perm}(\cdot, \mathbf{O}_2(\cdot, \cdot))$ and $\mathcal{L}_{state}(\cdot, \mathbf{O}_1^\sigma(\cdot, \cdot))$ respectively represent cardinality permutation and state losses, which are defined on the part of output layer of the neural network respectively representing the cardinality, $\alpha(\cdot, \cdot)$, the permutation, $\mathbf{O}_2(\cdot, \cdot)$, and the state of each of m_i set elements, $\mathbf{O}_1^\sigma(\cdot, \cdot)$ (*cf.* Fig. 1).

Implementation insight: In this scenario, for training neural network parameters \mathbf{w} , we need to jointly optimize three losses: cardinality $\mathcal{L}_{card}(\cdot, \alpha(\cdot, \cdot))$, permutation $\mathcal{L}_{perm}(\cdot, \mathbf{O}_2(\cdot, \cdot))$ and state $\mathcal{L}_{state}(\cdot, \mathbf{O}_1^\sigma(\cdot, \cdot))$, using SGD while the assignment (permutation) between ground truth annotations and the network outputs labels are unknown and interchangeable, which is sampled in each iteration by solving Eq. 9. Note that this equation is a discrete optimization to find the best permutation $\pi_{i,k}^*$, which can be solved using any independent discrete optimization approach depending on the choice of the objectives. In our paper, we use Hungarian (Munkres) algorithm.

Similar to **Scenario 1**, $\alpha(\cdot, \cdot)$ represents the parameters of the cardinality distribution (a discrete distribution) *i.e.* $\mathbf{O}_1 = (\mathbf{O}_1^1, \mathbf{O}_1^2, \dots, \mathbf{O}_1^M)$ are the state parts of the network output representing the collection of the states and existence score for all M set elements with the maximum size. For example in object detection, each \mathbf{O}_1^1 can simply represent parameters and existence for an axis-aligned bounding box, *e.g.* (x, y, w, h, s) . However, in contrast to **Scenario 1**, the assignment (permutation) between

ground truth annotations and the network outputs cannot be pre-fixed during training and they need to be deiced based on $\pi_{i,k}^*$ in each SGD iterations and for each input instance. Compared to **Scenario 1**, which is a proper set learning model for predicting a set of tags or category labels, this (and also the next scenario) is a proper model for learning to output a set of instances, *e.g.* bounding boxes, masks and trajectories, where the assignment between ground truth annotations and the network outputs can not be fixed; otherwise the network does not learn a sensible model for the task. We will validate this claim experimentally in Sec. 4.2.1.

In addition, in this scenario the outputs $\mathbf{O}_2(\cdot, \cdot)$ represent the parameters of another discrete distribution (the permutation distribution), where each discrete value in this distribution defines a unique permutation π of M set elements (the biggest set) and its ground truth for each input instance in each SGD iteration is attained from Eq. 9, *i.e.* $\pi_{i,k}^*$. Note that the ground truth annotations are assumed to be a set, *i.e.* we do not have any preference about their ordering or we do no have any prior knowledge if there is indeed any specific ordering structure in the annotations. By learning from the sampled permutations during SGD, we can have an extra information about the ordering structure of the annotations, *i.e.* there exist a single or multiple orders which matter or the problem is truly orderless.

3.2.3 Scenario 3: Order does not matter

This scenario is a special case of **Scenario 2** where the assignment (order) between the truth and the outputs can not be fixed during training step; However in this case, we do not consider learning the ordering structure (if exist any) in the annotations. For example, in the object detection problem, we may consider knowing the state of set of bounding boxes only, but ignoring how the bounding boxes are assigned (permuted) to the model output during training.

Therefore, in this case the distribution over the permutations, *i.e.* $p_m(\pi|\cdot, \cdot)$, can be assumed to be uniform, *i.e.* a normalized constant value for all permutations and all input instances,

$$p_m(\pi|\mathbf{x}_i, \mathbf{w}) = p_m(\pi) = \omega \quad \forall \pi \in \Pi \quad (11)$$

In this case, the posterior distribution in each SGD iteration (Eq. 8) is simplified as

$$\begin{aligned} p(\mathbf{w}_k|\mathcal{D}) &\approx \prod_{i=1}^n \left[p(m_i|\mathbf{x}_i, \mathbf{w}_k) \times U^{m_i} \times \omega \right. \\ &\quad \left. \times \prod_{\sigma=\pi_1}^{\pi_{m_i}} p(\mathbf{y}_\sigma|\mathbf{x}_i, \mathbf{w}_k, \pi_{i,k}^*) \right] p(\mathbf{w}_k), \end{aligned} \quad (12)$$

where $\pi_{i,k}^*$ is the best permutation sample for each instance i in each iteration of SGD k , attained by solving the following assignment problem:

$$\begin{aligned} \pi_{i,k}^* &= \arg \min_{\pi \in \Pi} -\log \left(\prod_{\sigma=\pi_1}^{\pi_{m_i}} p(\mathbf{y}_\sigma|\cdot, \cdot, \pi) \right) \\ &= \arg \min_{\pi \in \Pi} \sum_{\sigma=\pi_1}^{\pi_{m_i}} \mathcal{L}_{state}(\mathbf{y}_\sigma, \mathbf{O}_1^\sigma(\mathbf{x}_i, \mathbf{w}_{k-1})) \end{aligned} \quad (13)$$

To learn the parameters \mathbf{w} , the sampled permutation $\pi_{i,k}^*$ is used for back-propagation, *i.e.*

$$\begin{aligned}
\mathbf{w}_k &= \mathbf{w}_{k-1} - \eta \frac{-\partial \log(p(\mathbf{w}_{k-1}|\mathcal{D}))}{\partial \mathbf{w}_{k-1}} \\
&= \mathbf{w}_{k-1} - \eta \sum_{i=1}^n \left[\frac{\partial \mathcal{L}_{card}(m_i, \boldsymbol{\alpha})}{\partial \boldsymbol{\alpha}} \cdot \frac{\partial \boldsymbol{\alpha}}{\partial \mathbf{w}} + \right. \\
&\quad \left. \sum_{\sigma=\pi_1^*}^{\pi_m^*} \frac{\partial \mathcal{L}_{state}(\mathbf{y}_\sigma, \mathbf{O}_1^\sigma)}{\partial \mathbf{O}_1^\sigma} \cdot \frac{\partial \mathbf{O}_1^\sigma}{\partial \mathbf{w}} \right] + 2\gamma \mathbf{w}.
\end{aligned} \tag{14}$$

Implementation insight: The definition and implementations details for the outputs, *i.e.* $\boldsymbol{\alpha}(\cdot, \cdot)$ and $\mathbf{O}_1^\sigma(\cdot, \cdot)$ and their losses, *i.e.* $\mathcal{L}_{card}(\cdot, \boldsymbol{\alpha}(\cdot, \cdot))$, and $\mathcal{L}_{state}(\cdot, \mathbf{O}_1^\sigma(\cdot, \cdot))$ are identical to **Scenario 2**. The only difference is that the term $\mathcal{L}_{perm}(\cdot, \mathbf{O}_2(\cdot, \cdot))$ disappears from Eqs. 9 and 10.

Closely looking into Eqs. 9, 10, 13 and 14 in both **Scenarios 2 and 3** and considering $\mathcal{L}_{state}(\cdot, \cdot)$ only in these equations, this loss can be found under different names in the literature, *e.g.* Hungarian [41], Earth mover's and Chamfer [42] loss, where an assignment problem between the output of the network and ground truth needs be determined *before* the loss calculation and back-propagation. However, as explained in Eq. 7, these types of the losses are not actually permutation invariant losses and they are indeed a practical approximation for sampling (the best sample) from the permutation, as latent variable, in each SGD iteration.

3.3 Inference

The inference process for all three scenarios is identical because the inference is independent from the definition of the permutation distribution as shown below.

Having learned the network parameters \mathbf{w}^* , for a test input \mathbf{x}^+ , we use a MAP estimate to generate a set output, *i.e.* $\mathcal{Y}^* = \arg \min_{\mathcal{Y}} -\log(p(\mathcal{Y}|\mathcal{D}, \mathbf{x}^+, \mathbf{w}^*))$

$$\begin{aligned}
\mathcal{Y}^* &= \arg \min_{m, \mathcal{Y}^m} -\log(p(m|\mathbf{x}^+, \mathbf{w}^*)) - m \log U - \\
&\quad \log \sum_{\boldsymbol{\pi} \in \boldsymbol{\Pi}} \left(p_m(\boldsymbol{\pi}|\mathbf{x}^+, \mathbf{w}^*) \times \prod_{\sigma=\pi_1}^{\pi_m} p(\mathbf{y}_\sigma|\mathbf{x}^+, \mathbf{w}^*, \boldsymbol{\pi}) \right).
\end{aligned}$$

Note that in contrast to the learning step, the process how the set elements during the prediction step are sorted and represented, does not affect the output values. Another way to explain this is that the permutation is defined during training procedure only as it is applied on the ground truth labels for calculating the loss. Therefore, it does not affect the inference process. To this end, the product $\prod_{\sigma=\pi_1}^{\pi_m} p(\mathbf{y}_\sigma|\mathbf{x}^+, \mathbf{w}^*, \boldsymbol{\pi})$ is identical for any possible permutation, *i.e.* $\forall \boldsymbol{\pi} \in \boldsymbol{\Pi}$. Therefore, it can be factorized from the summation, *i.e.*

$$\begin{aligned}
&\log \sum_{\boldsymbol{\pi} \in \boldsymbol{\Pi}} \left(p_m(\boldsymbol{\pi}|\mathbf{x}^+, \mathbf{w}^*) \times \prod_{\sigma=\pi_1}^{\pi_m} p(\mathbf{y}_\sigma|\mathbf{x}^+, \mathbf{w}^*, \boldsymbol{\pi}) \right) \\
&= \log \left(\prod_{\sigma=1}^m p(\mathbf{y}_\sigma|\mathbf{x}^+, \mathbf{w}^*) \times \underbrace{\sum_{\boldsymbol{\pi} \in \boldsymbol{\Pi}} p_m(\boldsymbol{\pi}|\mathbf{x}^+, \mathbf{w}^*)}_{=1} \right) \\
&= \sum_{\sigma=1}^m \log(p(\mathbf{y}_\sigma|\mathbf{x}^+, \mathbf{w}^*)).
\end{aligned}$$

Therefore, the inference is simplified to

$$\begin{aligned}
\mathcal{Y}^* &= \arg \min_{m, \mathcal{Y}^m} -\log \left(\underbrace{p(m|\mathbf{x}^+, \mathbf{w}^*)}_{\boldsymbol{\alpha}} \right) - m \log U - \\
&\quad \sum_{\sigma=1}^m \log \left(\underbrace{p(\mathbf{y}_\sigma|\mathbf{x}^+, \mathbf{w}^*)}_{\mathbf{O}_1^\sigma} \right).
\end{aligned} \tag{15}$$

Implementation insight: Solving Eq. 15 corresponds to finding the optimal set $\mathcal{Y}^* = (m^*, \mathcal{Y}^{m^*})$, which is the **exact** solution of the problem. As shown in [8], this problem can be optimally and efficiently calculated using few simple operations, *e.g.* sorting, max and summation operations. Note that the unit of hyper-volume U is assumed as a constant hyper-parameter, tuned from the validation set of the data such that the best performance on this set is ensured.

An alternative to evaluate the models is an approximated inference [9], where the set cardinality is first approximated using $m^* = \text{argmin}_m -\log(p(m|\mathbf{x}^+, \mathbf{w}^*))$ and then all M set elements are sorted according to their existence scores and the state of top m^* set elements are shown as the final output. The main key difference between the exact and approximate inferences is in the calculation of finding the optimal cardinality, where the approximate inference finds m^* using the cardinality distribution only, while the exact inference considers all cardinality-related terms in Eq. 15, *i.e.* the cardinality distribution, hyper-parameter U and distribution over the existence scores of the set elements in order to calculate m^* .

4 EXPERIMENTAL RESULTS

To validate our proposed set learning approach, we perform experiments for each of the proposed scenarios including *i*) Multi-label image classification (**Scenario 1**), *ii*) object detection and identification on synthetic data (**Scenario 2**), *iii*) (a) pedestrian detection on real data and (b) a CAPTCHA test to partition a digit into its summands (**Scenario 3**).

4.1 Multi-label image classification (**Scenario 1**)

To validate the first learning model in Sec. 3.2.1 (**Scenario 1**), we perform experiments on the task of multi-label image classification. This is a suitable application as the output is expected to be in the form of a set, *i.e.* a set of category labels with an unknown cardinality while the order of its elements (category labels) in the output list does not have any preferable order. However, their order with respect to the network's output can be consistently fixed during training. Therefore, the best learning scheme for this application is **Scenario 1**, where the permutation is not a variable of the training process. To evaluate the framework, we use two standard public benchmarks for this problem, the PASCAL VOC 2007 dataset [46] and the Microsoft Common Objects in Context (MS COCO) dataset [47].

Implementation details. To train a network for predicting a set of tags for an image, we use the training scheme detailed as **Scenario 1**. To ensure a fair comparison with other works, we adopt the same base network architecture as [9], [19], [48], *i.e.* 16-layers VGG network [14] pretrained on the 2012 ImageNet dataset, as the backbone of our set prediction network. We adapt VGG for our purpose by modifying the last fully connected prediction layer to predict both cardinality $\boldsymbol{\alpha}(\cdot, \cdot)$ and the state of M set elements $\mathbf{O}_1 = (\mathbf{O}_1^1, \mathbf{O}_1^2, \dots, \mathbf{O}_1^M)$, which are only the existence scores for all M category labels in this problem. To train the model using Eq. 6, we define categorical distribution for cardinality and use softmax loss as \mathcal{L}_{card} and also binary cross-entropy (BCE) as \mathcal{L}_{card} . We then fine-tune the entire network using the training set of these datasets with the same train/test split as in existing literature [19], [48].

To optimize Eq. 6, we use stochastic gradient descent (SGD) and set the weight decay to $\gamma = 5 \cdot 10^{-4}$, with a momentum of 0.9

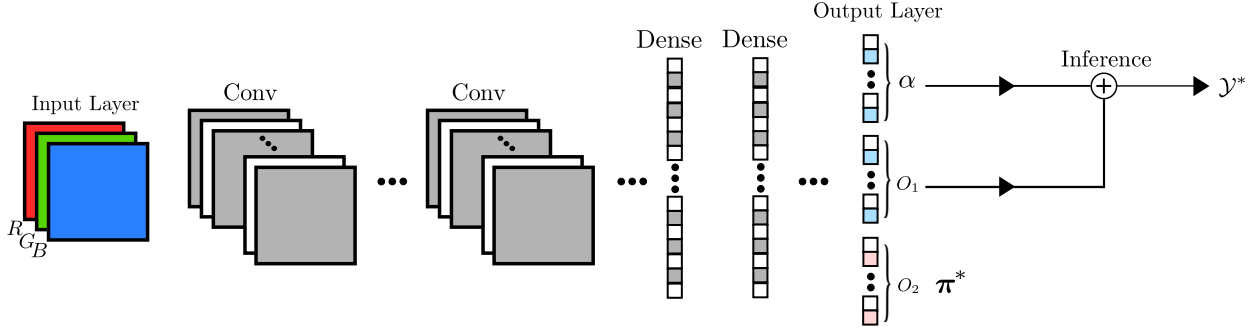


Fig. 1: A schematic overview of our Deep Perm-Set Network (**Scenario 2**). A structured input, *e.g.* an RGB image, is passed through a series of convolutional and fully connected layers with a collection of parameters denoted as w . The network architecture can be arbitrary and any widely used feed-forward architecture backbone, *e.g.* AlexNet [43], VGG [14], Resnet [44] or DenseNet [45], can be used. The output layer consists of three parts shown by α , \mathbf{O}_1 and \mathbf{O}_2 , which respectively predict the cardinality, the states and the permutation of the set elements. During training, $\pi_{i,k}^*$ representing a permutation sample (attained by Eq. 9), is used as the ground truth to update the loss $\mathcal{L}_{perm}(\pi_{i,k}^*, \mathbf{O}_2)$ and to sort the elements of the ground truth set's state in the $\mathcal{L}_{state}(\mathbf{Y}_{\pi_{i,k}^*}, \mathbf{O}_1)$ term in Eq. 10. During inference, the optimal set \mathcal{Y}^* is only calculated using the cardinality α and the states \mathbf{O}_1 outputs. π^* is an extra output for ordering representation. For **Scenarios 1 and 3**, the permutation head, *i.e.* \mathbf{O}_2 , is not defined.

and a dropout rate of 0.5. The learning rate is adjusted to gradually decrease after each epoch, starting from 0.001. The network is trained for 60 epochs for both datasets and the epoch with the lowest validation objective value is chosen for evaluation on the test set. The hyper-parameter U is set to be 2.36, adjusted on the validation set.

In our earlier work [9], we proposed the first set model based on **Scenario 1** only. However, we used two separate networks (two 16-layers VGG networks), one to model the set state (class scores) and one for cardinality. We also used the negative binomial as a cardinality loss. In addition, the trained model used approximate inference to generate the final set at test time. Here, we compare our proposed framework with the model from [9] to demonstrate the advantage of joint learning for each of the optimizing objectives, *i.e.* label's existence scores and their cardinality distribution. To ensure a fair comparison with [9], we add another baseline experiment where we use the same cardinality model but replace the negative binomial (NB) distribution used in [9] with the categorical distribution (Softmax). We follow the exact the same training protocol as [9] to train the classifier and cardinality network for the baseline approach.

Evaluation protocol. We employ the common evaluation metrics for multi-label image classification also used in [19], [48]. These include the average *precision*, *recall* and *F1-score*³ of the generated labels, calculated per-class (C-P, C-R and C-F1) and overall (O-P, O-R and O-F1). Since C-P, C-R and C-F1 can be biased to the performance of the most frequent classes, we also report the average *precision*, *recall* and *F1-score* of the generated labels per image/instance (I-P, I-R and I-F1).

We rely on F1-score to rank approaches on the task of label prediction. A method with better performance has a precision/recall value that has a closer proximity to the perfect point shown by the blue triangle in Fig. 2. To this end, for the classifiers such as BCE and Softmax, we find the optimal evaluation parameter $k = k^*$ that maximises the F1-score. For the set network model in [9] (DS) and our proposed framework with joint backbone network (JDS), prediction/recall is not dependent on the value of k . Rather, one single value for precision, recall and F1-score is computed.

3. F1-score is calculated as the harmonic mean of precision and recall.

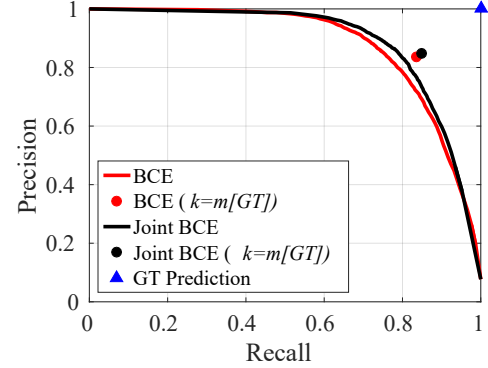


Fig. 2: Precision/recall curves for the classification scores when the classifier is trained independently (red solid line) and when it is trained jointly with the cardinality term using our proposed joint approach (black solid line) on PASCAL VOC dataset. The circles represent the upper bound when ground truth cardinality is used for the evaluation of the corresponding classifiers. The ground truth prediction is shown by a blue triangle.

PASCAL VOC 2007.

We first test our approach on the Pascal Visual Object Classes benchmark [46], which is one of the most widely used datasets for detection and classification. This dataset includes 9963 images with a 50/50 split for training and test, where objects from 20 pre-defined categories have been annotated by bounding boxes. Each image contains between 1 and 7 unique objects.

We first investigate if the learning using the shared backbone (joint learning) improves the performance of cardinality and classifier. Fig. 2 shows the precision/recall curves for the classification scores when the classifier is trained solely using binary cross-entropy (BCE) loss (red solid line) and when it is trained using the same loss jointly with the cardinality term (Joint BCE). We also evaluate the precision/recall values when the ground truth cardinality $m[GT]$ is provided. The results confirm our claim that the joint learning indeed improves the classification performance. We also calculate the mean absolute error of the cardinality estimation when the cardinality term using the DC loss is learned jointly and independently as in [9]. The mean absolute cardinality

TABLE 2: Quantitative results for multi-label image classification on the PASCAL VOC dataset.

Classifier	Eval.	C-P	C-R	C-F1	O-P	O-R	O-F1	I-P	I-R	I-F1
Softmax	$k=k^*(1)$	88.2	65.4	75.1	91.3	59.2	71.8	91.3	69.8	79.1
BCE	$k=k^*(1)$	88.7	58.6	70.5	92.2	59.8	72.5	92.2	70.1	79.6
DS (BCE-NB) [9]	$k=m^*$	76.8	74.8	75.8	80.6	76.7	78.6	83.4	81.9	82.6
DS (BCE-SftMx)	$k=m^*$	77.1	75.2	76.2	81.0	77.1	79.0	83.9	82.1	83.0
JDS (BCE-SftMx)	$k=m^*$	83.5	74.4	78.7	85.5	77.9	81.5	87.6	82.8	85.1

error of our prediction on PASCAL VOC is 0.31 ± 0.54 , while this error is 0.33 ± 0.53 when the cardinality is learned independently.

We compare the performance of our proposed set network, *i.e.* JDS (BCE-DC), with traditional learning approaches trained using classification losses only, *i.e.* softmax and BCE losses, while during the inference, the labels with the best k value are extracted as the model's output labels.

For the set based approaches, we included our model in [9] when the classifier is binary cross entropy and the cardinality loss is negative binomial, *i.e.* DS (BCE-NB). In addition, Table 2 reports the results for the deep set network when the cardinality loss is replaced by a categorical loss, *i.e.* (BCE-SftMx). The results show that we outperform the other approaches *w.r.t.* all three types of F1-scores. In addition, our joint formulation allows for a single training step to obtain the final model, while our model in [9] learns two VGG networks to generate the output sets.

Microsoft COCO.

The MS-COCO [47] benchmark is another popular benchmark for image captioning, recognition, and segmentation. The dataset includes 123K images, each labelled with per instance segmentation masks of 80 classes. The number of unique objects for each image varies between 0 and 18. Around 700 images in the training set do not contain any of the 80 classes and there are only a handful of images that have more than 10 tags. Most images contain between one and three labels. We use 82783 images with identical training and validation split as [9], and the remaining 40504 images as test data.

The classification results on this dataset are reported in Table 3. The results once again show that our approach consistently outperforms our traditional and set based baselines measured by F1-score. Our approach also outperform a recurrent based approach [19], which uses VGG-16 as the backbone along with a recurrent neural network to generate a set of labels. Due to this improvement, we achieve state-of-the-art results on this dataset as well. Some examples of label prediction using our proposed set network model and comparison with other deep set networks are shown in Fig. 3.

4.2 Object detection (Scenario 2 & 3)

Our second and third experiments are used to test our set formulation for the task of object detection using the model trained according to *i*) **Scenario 2** on synthetically generated data and *ii*) **Scenario 3** on real pedestrian data. We compare it with the state-of-the art object detectors, *i.e.* Faster-RCNN [22] and YOLO [21], [49]. To ensure a fair comparison, we use the exact same base network structure (ResNet-101) and the same training dataset. Moreover, the best hyper parameters, *e.g.* NMS threshold, are tuned for Faster-RCNN and YOLO detectors.

Formulation. We formulate object detection as a set prediction problem $\mathcal{Y} = \{\mathbf{y}_1, \dots, \mathbf{y}_m\}$, where each set element represents

a bounding box as $\mathbf{y} = (x_1, y_1, x_2, y_2, s) \in \mathbb{R}^5$, where (x_1, y_1) and (x_2, y_2) are respectively the top left and bottom right vertices of the bounding boxes and s represents an existence score for this set element.

Evaluation protocol. To quantify the detection performance, we adopt the commonly used evaluation curves and metrics [50] such as ROC, precision-recall curves, average precision (AP) and the log-average miss rate (MR) over false positive per image. Additionally, we compute the F1 score (the harmonic mean of precision and recall) for all competing methods.

4.2.1 Synthetic Data (Scenario 2)

Synthetic data generation. To evaluate our proposed object detector, we generate 55000 synthetic images with resolution 200x200 pixels, including 50000 images for training and 5000 for testing. For each synthetic image, we use a central crop of a randomly picked COCO 2014 image as background. The background images for our train and test sets were correspondingly taken from COCO 2014 train and validation sets in order to introduce less similarity between our train and test data. A random number of objects (from 0 to 4) is then rendered on the background. An object is a circle of radius r approximated by using Bézier curves, where r is randomly sampled between 25 and 50 pixels. Once the object has been created, random perturbations are applied on the control points of the curves in order to obtain a deformed ellipsoid as a result. Each object is either of red, green, yellow or blue color, with a certain variation of tone and brightness to simulate visual variations in natural images. To make the data more challenging, we allow severe overlap of the objects in the image - the intersection over union between a pair of object instances may be up to 85%. Also, random Gaussian noise is added to each image (See Figs. 4).

Training using Scenario 2. We train a convolutional neural network based on a standard ResNet-101 architecture, with loss heads directly attached to the the output of the ResNet. According to Eqs. 9 and 10, there are three main terms (losses) that need to be defined for this task. Firstly, the state loss $\mathcal{L}_{state}(\cdot)$ consists of two parts: *i*) Smooth L_1 -loss for the bounding box regression between the predicted output states and the permuted ground truth states, *ii*) Binary cross-entropy loss for the presence scores s . The ground truth score for a specific instance is 1 if it exists and 0 otherwise. The permutation using Eq. 10 is estimated approximately using Hungarian (Munkres) algorithm. Secondly, a categorical loss (Softmax) is used for the permutation $\mathcal{L}_{perm}(\cdot)$. Since this variable is not observable from the annotations, $\pi_{i,k}^*$ is calculated to estimate the ground truth permutation(s). Finally, for cardinality \mathcal{L}_{card} , a categorical loss is used in a similar fashion.

Results. Quantitative detection results on this dataset for Faster-RCNN, YOLO v3 and our proposed detector are shown in Tab. 4.

Our detector using the set formulation outperforms all other approaches *w.r.t.* all types of metrics. Considering the simplicity

TABLE 3: Quantitative results for multi-label image classification on the MS COCO dataset.

Classifier	Eval.	C-P	C-R	C-F1	O-P	O-R	O-F1	I-P	I-R	I-F1
Softmax	$k=k^*(3)$	58.6	57.6	58.1	60.7	63.3	62.0	60.7	74.7	67.0
BCE	$k=k^*(3)$	56.2	60.1	58.1	61.6	64.2	62.9	61.6	75.3	67.8
CNN-RNN [19]	$k=k^*(3)$	66.0	55.6	60.4	69.2	66.4	67.8	—	—	—
DS (Softmax-NB) [9]	$k=m^*$	68.2	59.9	63.8	68.8	67.4	68.1	74.3	72.6	73.5
DS (BCE-NB) [9]	$k=m^*$	66.5	62.9	64.6	70.1	68.7	69.4	75.2	73.6	74.4
DS (BCE-Sftmx)	$k=m^*$	68.0	61.7	64.7	72.4	67.1	69.6	76.0	73.3	74.6
JDS (BCE-Sftmx)	$k=m^*$	70.2	61.5	65.5	74.0	67.6	70.7	77.9	73.4	75.6

			
GT: person, skateboard	person, potted plant, remote	person, chair, handbag, umbrella	person, chair, dining table, bottle, cup, bowl, knife, fork, spoon, pizza
JDS: (BCE-SftMx)	person, skateboard	person, potted plant, remote	person, chair, dining table, bottle, cup, bowl, knife, fork, spoon, wine glass
DS: (BCE-SftMx)	person, baseball glove	person, chair , remote	person, chair, dining table, cup, bowl , book , knife, fork, wine glass
DS: (BCE-NB)	person, baseball glove , car	person, potted plant, chair , vase , remote	person, chair, dining table, cup, bowl , book , knife, fork

Fig. 3: Qualitative comparison between our proposed set network with a shared backbone (JDS) and the deep set networks with softmax (DS (BCE-Sftmx)) and Negative Binomial (DS (BCE-NB)) as the cardinality loss. For each image, the ground truth tags and the predictions for our JDS and the two baselines are denoted below. **False positives** are highlighted in red. Our JDS approach reduces both cardinality and classification error.

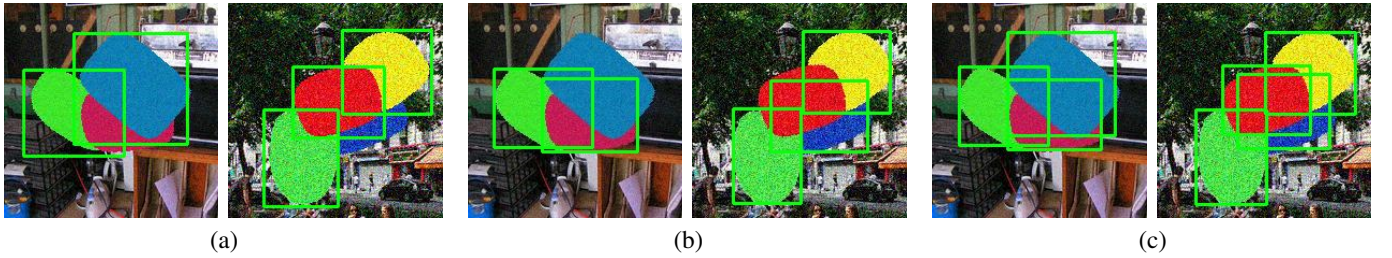


Fig. 4: A comparison between the detection performance of (a) Faster-RCNN, (b) YOLO v3 and (c) our set detector on heavily overlapping objects. Both Faster-RCNN and YOLO v3 fail to properly detect heavily occluded objects due to the required NMS heuristic. Please note that for Faster-RCNN and YOLO v3 the best NMS threshold, are tuned for this dataset.

TABLE 4: Detection results on the synthetic data measured by average precision, the best F1 scores (higher is better) and log-average miss rate (lower is better).

Method	AP \uparrow	F1-score \uparrow	MR \downarrow
Faster-RCNN	0.81	0.88	0.21
YOLO v3	0.86	0.91	0.17
Our Detector (w/o cardinality)	0.93	0.95	0.15
Our Detector	—	0.96	—

of the data and the very deep network used, *i.e.* ResNet-101, all methods work very well on localizing most of the objects with or without moderate partial occlusions. However, our set learning formulation naturally handles heavy occlusions (see Fig. 4) by outputting a set of detections with no heuristic involved.

Fig. 5(a) also shows the superior performance of our formula-

tion in detecting the objects with severe occlusion, quantitatively (about 20% improvement in F1 score compared to YOLO v3 and faster-RCNN for overlap level (IoU) above 0.5). The ROC and precision-recall curves for Faster-RCNN, YOLO v3 and our detector (w/o cardinality) are demonstrated in Fig. 5(b) and (c). Our approach outperforms other competing approaches with the highest F1-score and also the lowest miss rate given the same rate of false positives per image (for $0.08 \leq \text{fppi}$).

Detection & Identification results. In addition to the prediction of bounding boxes, our approach also provides the best ordering representation π^* for the bounding boxes for each input instance. In this dataset, this is equivalent to finding the association between bounding boxes belonging to similarly looking instances across the different images without any knowledge about this correspondence. For example, by testing three different images

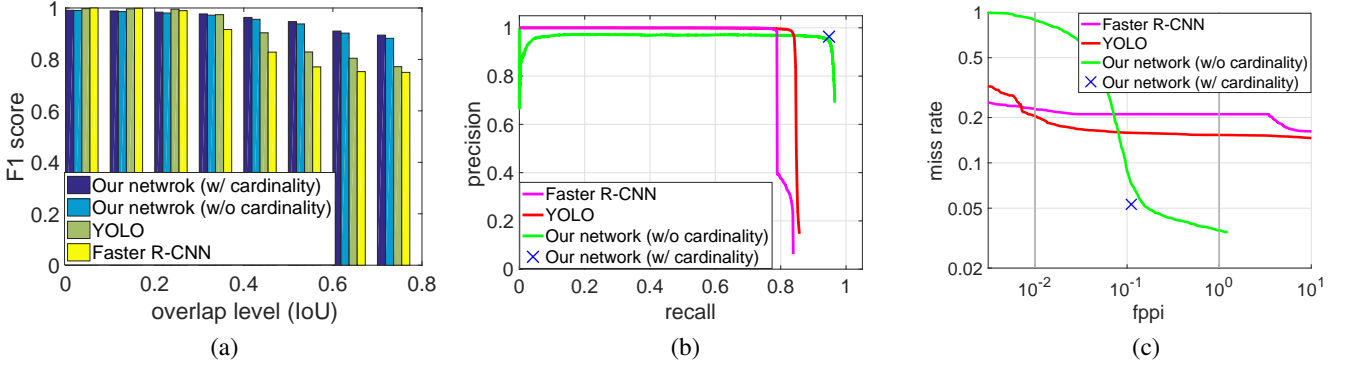


Fig. 5: (a) The best F1 scores against the level of object occlusions calculated by intersection of union (IoU), (b) Precision-Recall curve, and (c) ROC (miss rate-false positive per image) curve on synthetic data for the competing detectors: Faster-RCNN, YOLO v3, our network (w/o cardinality) and our network (w/ cardinality). Our final detection results are also shown as a single point in the curves.

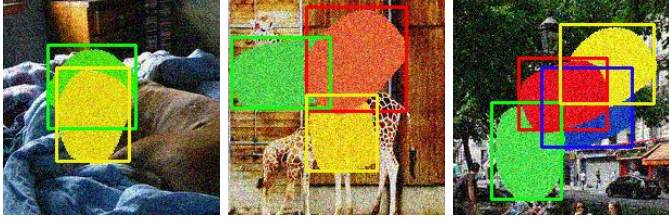


Fig. 6: The performance of our approach in detecting and also identifying the object instances using permutations. Here, box color uniquely identify corresponding objects.

in Fig 6, three sets of bounding boxes and their permutations, *e.g.* (2, 3), (2, 1, 3) and (3, 4, 2, 1), are predicted. If the bounding boxes are re-ordered according to their permutations in a descend or ascen order, each corresponding bounding boxes in each set will be associated to similar looking objects in each image. Therefore, we can simultaneously detect and identify visually similar instances in different test examples, *e.g.* in each frame of a video sequence.

For evaluation purposes only, we use the associations between similar looking objects which are available from our simulated data. For example, all bounding boxes belonging to the red object within the dataset with all its visual variations can be assumed to be the same instance. Therefore, we can evaluate our identification performance using this information. To assess the results, we use the permutation accuracy. We achieve 81.1% accuracy in identifying the objects. Fig. 6 shows the detection and identification results for three different images. Joint detection and identification of objects can be a fundamental step toward end-to-end training of a network for the multiple object tracking problem. However, the current formulation cannot handle large-scale object tracking problems due to the exponential number of permutations. Making the problem tractable for many targets, *e.g.* by an approximation for estimating a subset of dominant permutations, and incorporating motions is left for future work.

An additional baseline experiment. We performed an additional baseline experiment by training the set network using **Scenario 1** with the same base network structure (ResNet-101) on the synthetic data reported above. In contrast to the losses for the model trained using **Scenario 2**, (Fig. 7 (a)), the training and validation losses for the model trained using **Scenario 1** (Fig. 7 (b)) cannot decrease beyond a very high value and the generated boxes are simply an average of the positions and sizes (Fig. 8), proving the ineffectiveness of this training scheme to learn a reasonable model for this task. As mentioned before, the reason for this failure is that

the permutations are not considered in **Scenario 1**. Therefore, when the network is trained with orderless outputs such as bounding boxes, the model is confused. Thus, its objective function does not converge when forcing it to learn from such data.

4.2.2 Real data (Scenario 3)

Dataset. We use training sequences from *MOTChallenge* pedestrian detection and tracking benchmark, *i.e.* 2DMOT2015 [51] and MOT17Det [52], to create our dataset. Each sequence is split into train and test sub-sequences, and the images are cropped on different scales so that each crop contains up to 5 pedestrians. Our aim is to show the main weakness of the existing object detectors, *i.e.* the heuristics used for handling partial occlusions, which is crucial in problems like multiple object tracking and instance level segmentation. To this end, we only evaluate the approaches on small-scale data (up to 5 objects) which include a single type of objects, *e.g.* pedestrian, with high level of occlusions. The resulting dataset has 50K training and 5K test samples.

Training using Scenario 3. We train a convolutional neural network based on a standard ResNet-101 architecture, with loss heads directly attached to the the output of ResNet. According to Eqs. (13, 14), there are two main terms (losses) that need to be defined for this task. Firstly, the state loss $\mathcal{L}_{state}(\cdot)$ consists of two parts: *i*) Smooth L_1 -loss for the bounding box regression between the predicted output states and the permuted ground truth states, *ii*) Binary cross-entropy loss for the presence scores s . The ground truth score for a specific instance is 1 if it exists and 0 otherwise. The permutation is estimated iteratively using alternation according to Eq. (13) using Hungarian (Munkres) algorithm. Secondly, for cardinality $\mathcal{L}_{card}(\cdot)$, a categorical loss (Softmax) is used as the distcete distribution model.

For training we use Adam optimizer with learning rate of 0.001, $\beta_1 = 0.9$, $\beta_2 = 0.999$ and $\epsilon = 10^{-8}$. To accelerate and stabilize the training process, batch normalization is employed and a weight decay of 0.0001 was used as an additional regularization term. The hyper-parameter U is set to be 0.1, adjusted on the validation set.

Detection results. Quantitative detection results for Faster-RCNN, YOLO v3 and our proposed detector are shown in Tab. 5. Since our detector generates a single set only (a set of bounding boxes) using the inference introduced in Sec. 3.3, there exists one single value for precision-recall and thus F1-score. For this reason, the average precision (AP) and log-average miss rate (MR) calculated over different thresholds cannot be reported in this case. To this end, we report these values on our approach using the

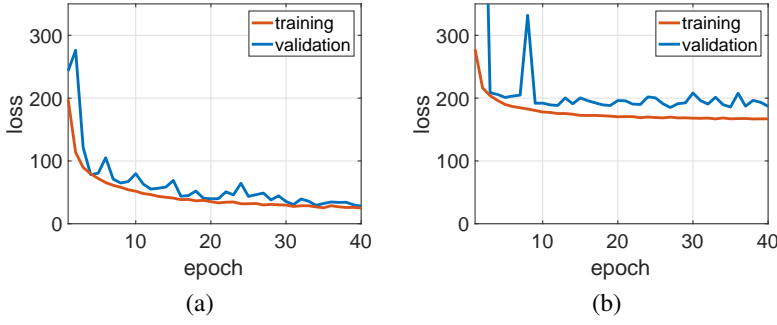


Fig. 7: Training and validation losses of the model trained using (a) **Scenario 2** and (b) **Scenario 3**, for object detection task.

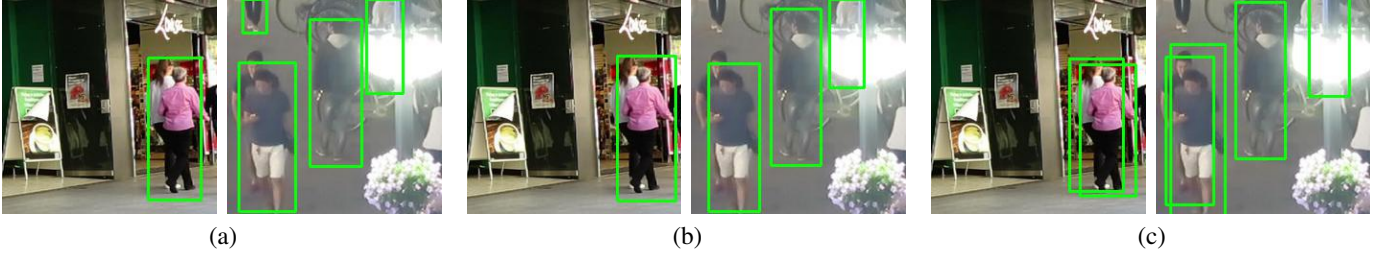


Fig. 9: A comparison between the detection performance of (a) Faster-RCNN, (b) YOLO v3 and (c) our set detector on heavily overlapping pedestrians from *MOTChallenge* benchmark. Both Faster-RCNN and YOLO v3 fail to properly detect heavily occluded pedestrians due to NMS.

TABLE 5: Detection results on the real data measured by average precision, the best F1 scores (higher is better) and log-average miss rate (lower is better).

Method	AP \uparrow	F1-score \uparrow	MR \downarrow	Time (ms) \downarrow
Faster-RCNN	0.68	0.76	0.48	101.0
YOLO v3	0.70	0.76	0.48	18.2
Our Detector (w/o card.)	0.75	0.80	0.47	15.1
Our Detector	—	0.80	—	15.1

predicted boxes with their scores only, and ignore the cardinality term and the inference step. To ensure a fair comparison, the F1-score reported in this table reflects the best score for Faster-RCNN and YOLO v3 along the precision-recall curve. Quantitative results in Tab. 5 show that our detector using the set formulation significantly outperforms all other approaches on all metrics.

We further investigate failure cases for Faster-RCNN and YOLO v3 in Fig. 9. In case of heavy occlusions, the conventional formulation of both methods, which include the NMS heuristics, is not capable of correctly detecting all objects, *i.e.* pedestrians. Note that lowering the overlapping threshold in NMS in order to tolerate a higher level of occlusion results in more false positives for each object. In contrast, more occluding objects are miss-detected by increasing the value of this threshold. Therefore, changing the overlap threshold for NMS heuristics would not be conducive for improving their detection performances.

In contrast, our set learning formulation naturally handles heavy occlusions (see Fig. 9) by outputting a set of detections with no heuristic involved. Fig. 10(a) also shows the superior performance of our formulation in detecting the objects with severe occlusion. Our method has an improvement of 5-15% in F1 score compared to YOLO v3 and Faster-RCNN for high overlap level (IoU) between 0.3–0.7. The overall performance ROC and precision-recall curves for Faster-RCNN, YOLO v3 and our detector (w/o cardinality) are shown in Fig. 10(b) and (c). Note, that the single point in these curves represents our final detection result. Our approach outperforms other competing approaches with the highest F1-score

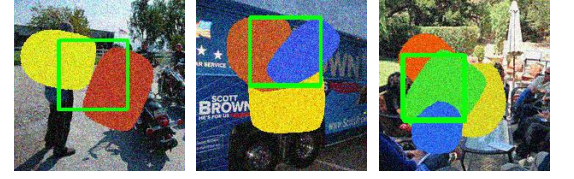


Fig. 8: The predicted bounding boxes from the network trained using **Scenario 1**, when trained for the object detection task. In all images, all the bounding boxes are concentrated in the same location with the exactly same size, which are simply an average of all the positions and sizes of the objects in the scene.

and also the lowest miss rate given the same rate of false positives per image. This is significant as our set network is not yet well-developed for the detection task while YOLO v3 and Faster-RCNN are well engineered for this application.

We also report the inference time for all detectors in Tab. 5. Since our detector, similar to YOLO v3, is a single stage detector, it is significantly faster than Faster-RCNN and marginally faster than YOLO v3 as it does not need the post-processing step, *i.e.* NMS.

4.3 CAPTCHA test for de-summing a digit (Scenario 3)

We also evaluate our set formulation on a CAPTCHA test where the aim is to determine whether a user is a human or not by a moderately complex logical test. In this test, the user is asked to decompose a *query digit* shown as an image (Fig. 11 (left)) into a set of digits by clicking on a subset of numbers in a noisy image (Fig. 11 (right)) such that the summation of the selected numbers is equal to the *query digit*.

In this puzzle, it is assumed there exists only one valid solution (including an empty response). We target this complex puzzle with our set learning approach. What is assumed to be available as the training data is a set of spotted locations in the *set of digits* image and no further information about the represented values of *query digit* and the *set of digits* is provided. In practice, the annotation can be acquired from the users' click when the test is successful. In our case, we generate a dataset for this test from the real handwriting MNIST dataset.

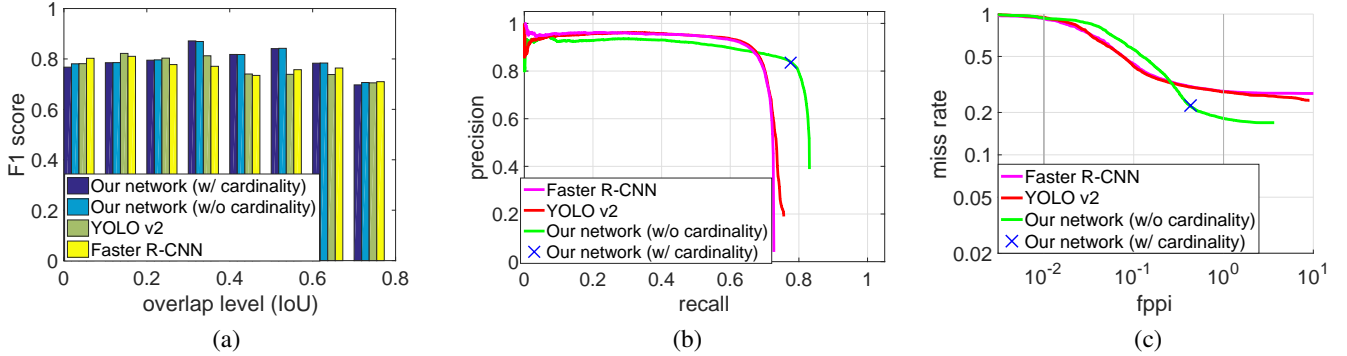


Fig. 10: (a) The best F1 scores against the level of object occlusions calculated by intersection of union (IoU), (b) Precision-Recall curve, and (c) ROC (miss rate-false positive per image) curve on pedestrian detection data for the competing detectors: Faster-RCNN, YOLO v3, our network (w/o cardinality) and our network (w/ cardinality). Our final detection results are also shown as a single point in the curves.



Fig. 11: A *query digit* (left) and a *set of digits* (right) for the proposed CAPTCHA test. The ground truth and our predicted solutions are shown by white and red boxes respectively.

Data generation. The dataset is generated using the MNIST dataset of handwritten digits. The *query digit* is generated by randomly selecting one of the digits from MNIST dataset. Given a *query digit*, we create a series of random digits with different length such that there exists a subset of these digits that sums up to the *query digit*. Note that in each instance there is only one solution (including empty) to the puzzle. We place the chosen digits in a random position on a 300×75 blank image with different rotations and sizes. To make the problem more challenging, random white noise is added to both the *query digit* and the *set of digits* images (Fig. 11). The produced dataset includes 100K problem instances for training and 10K images for evaluation, generated independently from MNIST training and test sets.

Baseline methods. Considering the fact that only a set of locations is provided as ground truth, this problem can be seen as an analogy to the object detection problem. However, the key difference between this logical test and the object detection problem is that the objects of interest (the selected numbers) change as the *query digit* changes. For example, in Fig. 11, if the *query digit* changes to another number, *e.g.* 4, the number $\{4\}$ should be only chosen. Thus, for the same *set of digits*, now $\{1, 2, 5\}$ would be labeled as background. Since any number can be either background or foreground conditioned on the *query digit*, this problem cannot be trivially formulated as an object detection task. To prove this claim, as a baseline, we attempt to solve the CAPTCHA problem using a detector, *e.g.* Faster-RCNN, with the same base structure as our network (ResNet-101) and trained on the exactly same data including the *query digit* and the *set of digits* images⁴.

As an additional baseline, we also present a solution to this set problem using a recurrent model, very similar to the framework proposed in [10]. To this end, we feed the inputs to the same base structure as our network (ResNet-101) and replace the last

4. To ensure inputting one single image into the ResNet-101 backbone, we represent both the *query digit* and the *set of digits* by a single image such that the *query digit* always appears in the bottom left corner of the *set of digits* image (See Figs 13 and 14).

TABLE 6: Accuracy for solving the CAPTCHA test.

Faster-RCNN	LSTM+Hungarian	Ours
26.8%	66.1%	95.6%

fully connected layer with a one layer LSTM, which is used to predict in each iteration the parameters of a bounding box, *i.e.* $\mathbf{y} = (x_1, y_1, x_2, y_2, s)$. During training, we use Hungarian algorithm to match the predicted bounding boxes with the ground truths. During inference, the predicted bounding boxes with a score above 0.5 are represented as the final outputs.

Implementation details. We use the same set formulation as in the previous experiment on object detection. Similarly, we train the same network structure (ResNet-101) using the same optimizer and hyper-parameters as described in 4.2. Similar to the previous experiment, we do not use the permutation loss $\mathcal{L}_{perm}(\cdot)$ (**Scenario 2**) since we are not interested in the permutation distribution of the detected digits in this experiment. However, we still need to estimate the permutations iteratively using Eq. 13 to permute the ground truth for $\mathcal{L}_{state}(\cdot)$.

The input to the network is both the *query digit* and the *set of digits* images and the network outputs bounding boxes corresponding to the solution set. The hyper-parameter U is set to be 2, adjusted on the validation set.

Evaluation protocol. Localizing the numbers that sum up to the query digit is important for this task, therefore, we evaluate the performance of the network by comparing the ground truth with the predicted bounding boxes. More precisely, to represent the degree of match between the prediction and ground truth, we employ the commonly used Jaccard similarity coefficient. If $IoU_{(b_1, b_2)} > 0.5$ for all the numbers in the solution set, we mark the instance as correct otherwise the problem instance is counted as incorrect.

Results. The accuracy for solving this test using all competing methods is reported in Tab. 6. As expected, Faster-RCNN fails to solve this test and achieves an accuracy of 26.8%. This is because Faster-RCNN only learns to localize digits in the image and ignores the logical relationship between the objects of interest. A detection framework is not capable of performing reasoning in order to generate a sensible score for a subset of objects (digits). The LSTM+ Hungarian network is able to approximate the mapping between inputs and the outputs as it can be trained in an end-to-end fashion. However, it is worse than our approach at solving this problem, mainly due to the assumption about sequential dependency between the outputs (even with an

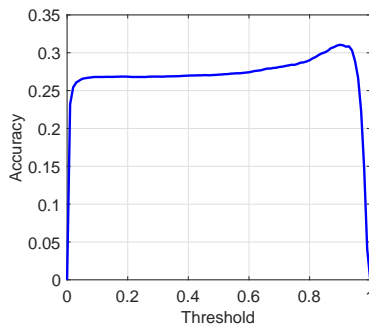


Fig. 12: A plot, representing the accuracy of solving the CAPTCHA test using Faster-RCNN against the detection threshold.

unknown ordering/permuation), which is not always satisfied in this experiment. In contrast, our set prediction formulation provides an accurate model for this problem and gives the network the ability of mimicking arithmetic implicitly by end-to-end learning the relationship between the inputs and outputs from the training data. In fact, the set network is able to generate different sets with different states and cardinality if one or both of the inputs change. This shows the potential of our formulation to tackle arithmetical, logical or semantic relationship problems between inputs and output sets without any explicit knowledge about arithmetic, logic or semantics.

For solving the CAPTCHA test using Faster-RCNN, we investigated if changing the detection threshold can improve the accuracy of the test. As shown in Fig. 12, this threshold has a slight effect on the test accuracy, increasing it from 26.8% for a default detection threshold of 0.5 to 31.05% for the optimal threshold.

We also explored if an additional network, trained to recognize the digits, can be used in combination with Faster-RCNN in order to improve the accuracy of the test. To this end, we used another ResNet-101 network and trained in MNIST dataset to recognise the digits. Note that we assumed that the annotations for our dataset are only the bounding boxes and no information about the *query digit* and the *set of digits* are provided. Therefore, this new classifier network could not be trained on our dataset.

In order to solve the test with an additional digit classifier, both the *query digit* and the detected numbers from Faster-RCNN are fed to the classifier network to recognise their values. Then, a subset of the detected digits (including an empty set) is chosen to solve the test. It is obvious that the test accuracy is affected by the performance of both detection and classifier networks. For this experiment, the test accuracy is increased considerably from **31.05%** to **59.28%**. However, it is still significantly beyond our reported results for this test (**95.2%**).

Figure 13 shows more results from our approach to solve this test. The output of Faster-RCNN for the examples are also shown in Figure 14.

5 CONCLUSION

In this paper, we proposed a framework for predicting sets with unknown cardinality and permutation using convolutional neural networks. In our formulation, set permutation is considered as an unobservable variable and its distribution is estimated iteratively using alternating optimization. We have shown that object detection can be elegantly formulated as a set prediction problem, where a deep network can be learned end-to-end to generate the detection

outputs with no heuristic involved. We have demonstrated that the approach is able to outperform the state-of-the art object detections on real data including highly occluded objects. We have also shown the effectiveness of our set learning approach on solving a complex logical CAPTCHA test, where the aim is to de-sum a digit into its components by selecting a set of digits with an equal sum value.

The main limitation of the current framework is that the number of possible permutations exponentially grows with the maximum set size (cardinality). Therefore, applying it to large-scale problem is not straightforward and requires an accurate approximation for estimating a subset of dominant permutations. In future, we plan to overcome this limitation by learning the subset of significant permutations to target real-world large-scale problems such as multiple object tracking.

REFERENCES

- [1] A. Krizhevsky, I. Sutskever, and G. E. Hinton, “ImageNet classification with deep convolutional neural networks,” in *NIPS*2012*, pp. 1097–1105.
- [2] G. Papandreou, L.-C. Chen, K. P. Murphy, and A. L. Yuille, “Weakly- and semi-supervised learning of a deep convolutional network for semantic image segmentation,” Dec. 2015.
- [3] G. Hinton, L. Deng, D. Yu, G. E. Dahl, A.-r. Mohamed, N. Jaitly, A. Senior, V. Vanhoucke, P. Nguyen, T. N. Sainath *et al.*, “Deep neural networks for acoustic modeling in speech recognition: The shared views of four research groups,” *IEEE Signal Processing Magazine*, vol. 29, no. 6, pp. 82–97, 2012.
- [4] V. Mnih, K. Kavukcuoglu, D. Silver, A. Graves, I. Antonoglou, D. Wierstra, and M. Riedmiller, “Playing atari with deep reinforcement learning,” *arXiv preprint arXiv:1312.5602*, 2013.
- [5] V. Mnih, K. Kavukcuoglu, D. Silver, A. A. Rusu, J. Veness, M. G. Bellemare, A. Graves, M. Riedmiller, A. K. Fidjeland, G. Ostrovski *et al.*, “Human-level control through deep reinforcement learning,” *Nature*, vol. 518, no. 7540, pp. 529–533, 2015.
- [6] J. Johnson, A. Karpathy, and L. Fei-Fei, “Densecap: Fully convolutional localization networks for dense captioning,” 2016.
- [7] M. Zaheer, S. Kottur, S. Ravanbakhsh, B. Poczos, R. Salakhutdinov, and A. Smola, “Deep sets,” in *NIPS*, 2017.
- [8] S. H. Rezatofighi, A. Milan, Q. Shi, A. Dick, and I. Reid, “Joint learning of set cardinality and state distribution,” in *AAAI*, 2018.
- [9] S. H. Rezatofighi, V. K. BG, A. Milan, E. Abbasnejad, A. Dick, and I. Reid, “Deepsetnet: Predicting sets with deep neural networks,” in *ICCV*, 2017.
- [10] O. Vinyals, S. Bengio, and M. Kudlur, “Order matters: Sequence to sequence for sets,” *ICLR*, 2015.
- [11] R. L. Murphy, B. Srinivasan, V. Rao, and B. Ribeiro, “Janossy pooling: Learning deep permutation-invariant functions for variable-size inputs,” in *ICLR*.
- [12] K. Skianis, G. Nikolentzos, S. Limnios, and M. Vaziriannis, “Rep the set: Neural networks for learning set representations,” *arXiv preprint arXiv:1904.01962*, 2019.
- [13] Y. Zhang, J. Hare, and A. Prügel-Bennett, “Deep set prediction networks,” in *NeurIPS*, 2019.
- [14] K. Simonyan and A. Zisserman, “Very deep convolutional networks for large-scale image recognition,” *CoRR*, vol. abs/1409.1556, 2014. [Online]. Available: <https://arxiv.org/pdf/1409.1556.pdf>
- [15] C. Szegedy, W. Liu, Y. Jia, P. Sermanet, S. Reed, D. Anguelov, D. Erhan, V. Vanhoucke, and A. Rabinovich, “Going deeper with convolutions,” *CoRR*, vol. abs/1409.4842, 2014. [Online]. Available: <http://arxiv.org/abs/1409.4842>
- [16] K. He, X. Zhang, S. Ren, and J. Sun, “Deep residual learning for image recognition,”
- [17] O. Russakovsky, J. Deng, H. Su, J. Krause, S. Satheesh, S. Ma, Z. Huang, A. Karpathy, A. Khosla, M. Bernstein, A. C. Berg, and L. Fei-Fei, “Imagenet large scale visual recognition challenge,” *IJCV*, vol. 115, no. 3, pp. 211–252, 2015.
- [18] Y. Gong, Y. Jia, T. Leung, A. Toshev, and S. Ioffe, “Deep convolutional ranking for multilabel image annotation,” *arXiv preprint arXiv:1312.4894*, 2013.
- [19] J. Wang, Y. Yang, J. Mao, Z. Huang, C. Huang, and W. Xu, “CNN-RNN: A unified framework for multi-label image classification,” in *CVPR*.
- [20] J. Redmon, S. Divvala, R. Girshick, and A. Farhadi, “You only look once: Unified, real-time object detection,” in *Proc. IEEE Conf. Comput. Vis. Patt. Recogn. (CVPR)*, 2016, pp. 779–788.

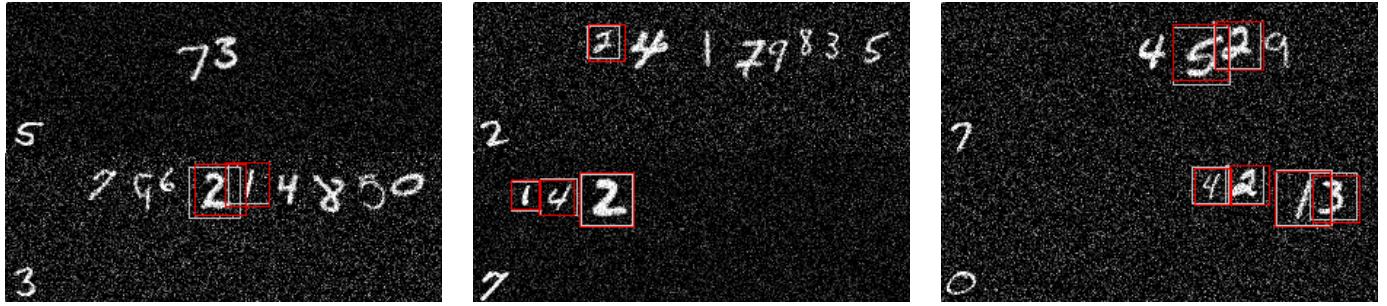


Fig. 13: Further examples showing a perfect prediction of the solution using our Deep Perm-Set Network. Each image contains a *query digit* (bottom left corner) and a *set of digits*. The ground truth and our predicted solutions are shown by white and red boxes respectively. Note that zero represents number 10 for our experiment.

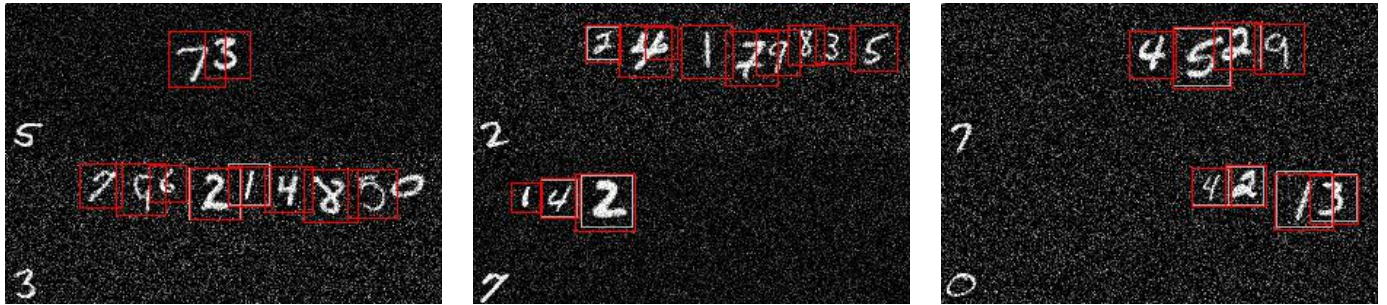


Fig. 14: Further examples showing the solution of Faster-RCNN for the test. Each image contains a *query digit* (bottom left corner) and a *set of digits*. The ground truth and the predicted solutions for Faster-RCNN are shown by white and red boxes respectively. Faster-RCNN simply learns to detect almost all the digits while ignoring the logical relationship between the *query digit* and the *set of digits*.

- [21] J. Redmon and A. Farhadi, “Yolo9000: better, faster, stronger,” in *Proc. IEEE Conf. Comput. Vis. Patt. Recogn. (CVPR)*, 2017.
- [22] S. Ren, K. He, R. Girshick, and J. Sun, “Faster r-cnn: Towards real-time object detection with region proposal networks,” in *NIPS*, 2015, pp. 91–99.
- [23] J. Hosang, R. Benenson, and B. Schiele, “Learning non-maximum suppression,” in *CVPR*, 2017.
- [24] Y. Liu, L. Liu, H. Rezatofighi, T.-T. Do, Q. Shi, and I. Reid, “Learning pairwise relationship for multi-object detection in crowded scenes,” *arXiv preprint arXiv:1901.03796*, 2019.
- [25] D. M. Blei, A. Y. Ng, and M. I. Jordan, “Latent dirichlet allocation,” *Journal of machine Learning research*, vol. 3, no. Jan, pp. 993–1022, 2003.
- [26] C. R. Qi, H. Su, K. Mo, and L. J. Guibas, “Pointnet: Deep learning on point sets for 3d classification and segmentation,” in *CVPR*, 2017, pp. 652–660.
- [27] C. R. Qi, L. Yi, H. Su, and L. J. Guibas, “Pointnet++: Deep hierarchical feature learning on point sets in a metric space,” in *NeurIPS*, 2017, pp. 5099–5108.
- [28] L. P. Tchapmi, V. Kosaraju, H. Rezatofighi, I. Reid, and S. Savarese, “TopNet: Structural point cloud decoder,” in *CVPR*, 2019, pp. 383–392.
- [29] T.-Y. Lin, M. Maire, S. Belongie, J. Hays, P. Perona, D. Ramanan, P. Dollár, and C. L. Zitnick, “Microsoft coco: Common objects in context,” in *IEEE Europ. Conf. Comput. Vision (ECCV)*, 2014, pp. 740–755.
- [30] B. Babenko, M.-H. Yang, and S. Belongie, “Robust object tracking with online multiple instance learning,” *IEEE transactions on pattern analysis and machine intelligence*, vol. 33, no. 8, pp. 1619–1632, 2011.
- [31] A. Alahi, K. Goel, V. Ramanathan, A. Robicquet, L. Fei-Fei, and S. Savarese, “Social lstm: Human trajectory prediction in crowded spaces,” in *CVPR*, 2016, pp. 961–971.
- [32] A. Sadeghian, V. Kosaraju, A. Sadeghian, N. Hirose, H. Rezatofighi, and S. Savarese, “Sophie: An attentive gan for predicting paths compliant to social and physical constraints,” in *CVPR*, 2019, pp. 1349–1358.
- [33] L. A. Hannah, D. M. Blei, and W. B. Powell, “Dirichlet process mixtures of generalized linear models,” *Journal of Machine Learning Research*, vol. 12, no. Jun, pp. 1923–1953, 2011.
- [34] N.-Q. Tran, B.-N. Vo, D. Phung, and B.-T. Vo, “Clustering for point pattern data,” in *ICPR*. IEEE, 2016, pp. 3174–3179.
- [35] K. Muandet, K. Fukumizu, F. Dinuzzo, and B. Schölkopf, “Learning from distributions via support measure machines,” in *NIPS*, 2012, pp. 10–18.
- [36] J. Oliva, B. Póczos, and J. Schneider, “Distribution to distribution regression,” in *ICML*, 2013, pp. 1049–1057.
- [37] B.-N. Vo, D. Phung, Q. N. Tran, and B.-T. Vo, “Model-based multiple instance learning,” *arXiv*, 2017.
- [38] B.-N. Vo, N.-Q. Tran, D. Phung, and B.-T. Vo, “Model-based classification and novelty detection for point pattern data,” in *ICPR*. IEEE, 2016, pp. 2622–2627.
- [39] R. P. Adams, I. Murray, and D. J. MacKay, “Tractable nonparametric bayesian inference in poisson processes with gaussian process intensities,” in *ICML*, 2009, pp. 9–16.
- [40] S. H. Rezatofighi, R. Kaskman, F. T. Motlagh, Q. Shi, D. Cremers, L. Leal-Taixé, and I. Reid, “Deep perm-set net: learn to predict sets with unknown permutation and cardinality using deep neural networks,” *arXiv preprint arXiv:1805.00613*, 2018.
- [41] R. Stewart and M. Andriluka, “End-to-end people detection in crowded scenes,” *arXiv:1506.04878 [cs]*, Jun. 2015, arXiv: 1506.04878. [Online]. Available: <http://arxiv.org/abs/1506.04878>
- [42] H. Fan, H. Su, and L. J. Guibas, “A point set generation network for 3d object reconstruction from a single image,” in *CVPR*, 2017, pp. 605–613.
- [43] A. Krizhevsky, I. Sutskever, and G. E. Hinton, “Imagenet classification with deep convolutional neural networks,” in *NeurIPS*, 2012, pp. 1097–1105.
- [44] K. He, X. Zhang, S. Ren, and J. Sun, “Deep residual learning for image recognition,” in *CVPR*, 2016, pp. 770–778.
- [45] G. Huang, Z. Liu, L. Van Der Maaten, and K. Q. Weinberger, “Densely connected convolutional networks,” in *CVPR*, 2017, pp. 4700–4708.
- [46] M. Everingham, L. Van Gool, C. K. I. Williams, J. Winn, and A. Zisserman, *The PASCAL Visual Object Classes Challenge 2007 (VOC2007) Results*. [Online]. Available: <http://www.pascal-network.org/challenges/VOC/voc2007/workshop/index.html>
- [47] T.-Y. Lin, M. Maire, S. Belongie, L. Bourdev, R. Girshick, J. Hays, P. Perona, D. Ramanan, C. L. Zitnick, and P. Dollár, “Microsoft COCO: Common objects in context,” *arXiv:1405.0312 [cs]*, May 2014, arXiv: 1405.0312. [Online]. Available: <http://arxiv.org/abs/1405.0312>
- [48] Y. Gong, Y. Jia, T. Leung, A. Toshev, and S. Ioffe, “Deep convolutional ranking for multilabel image annotation,” *CoRR*, vol. abs/1312.4894, 2013. [Online]. Available: <http://arxiv.org/abs/1312.4894>
- [49] J. Redmon and A. Farhadi, “Yolov3: An incremental improvement,” *arXiv preprint arXiv:1804.02767*, 2018.

- [50] P. Dollár, C. Wojek, B. Schiele, and P. Perona, “Pedestrian detection: An evaluation of the state of the art,” *PAMI*, vol. 34, 2012.
- [51] L. Leal-Taixé, A. Milan, I. D. Reid, S. Roth, and K. Schindler, “Motchallenge 2015: Towards a benchmark for multi-target tracking,” *CoRR*, vol. abs/1504.01942, 2015.
- [52] A. Milan, L. Leal-Taixé, I. D. Reid, S. Roth, and K. Schindler, “MOT16: A benchmark for multi-object tracking,” *CoRR*, vol. abs/1603.00831, 2016.